Journal Pre-proofs

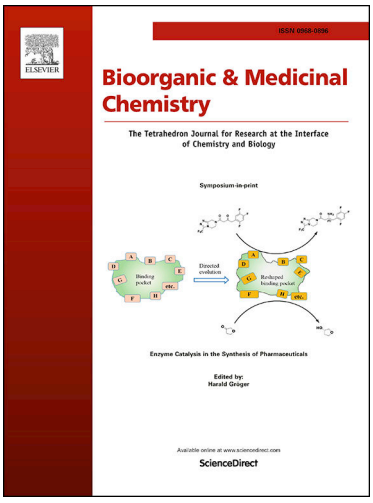

Synthesis and biological evaluation of NQO1-activated prodrugs of podophyllotoxin as antitumor agents

Yan Qu, Chong Zhang, Xin Ma, Yunhui Gao, Jing Liu, Liqiang Wu

PII: S0968-0896(20)30651-9
DOI: https://doi.org/10.1016/j.bmc.2020.115821
Reference: BMC 115821

To appear in: *Bioorganic & Medicinal Chemistry*

Received Date: 2 September 2020
Accepted Date: 5 October 2020

Please cite this article as: Y. Qu, C. Zhang, X. Ma, Y. Gao, J. Liu, L. Wu, Synthesis and biological evaluation of NQO1-activated prodrugs of podophyllotoxin as antitumor agents, *Bioorganic & Medicinal Chemistry* (2020), doi: https://doi.org/10.1016/j.bmc.2020.115821

Synthesis and biological evaluation of NQO1-activated prodrugs of podophyllotoxin as antitumor agents

Yan Qu [a, 1], Chong Zhang[b,c,1], Xin Ma[b], Yunhui Gao[b], Jing Liu[b], Liqiang Wu[b,*]

[a]*School of Basic Medical Sciences, Xinxiang Medical University, Xinxiang 453003, China.*

[b]*School of Pharmacy, Xinxiang Medical University, Xinxiang 453003, China*

[c]*Department of Pharmacology, Xi'an Jiaotong University School of Medicine, 76 West Yanta Road, Xi'an 710061, China.*

**Corresponding author. E-mail: wliq1974@163.com*

[1]*Co first-authors*

ABSTRACT Podophyllotoxin (PPT), a toxic polyphenol derived from the roots of genus Podophyllum, had been reported with strong inhibition on both normal human cells and tumor cells, which hindered the development of PPT as the candidate antitumor agent. In the present work, multiple NQO1-activatable PPT prodrugs were synthesized for reducing normal cell toxicity and keeping tumor cell toxicity. The antiproliferative activities in vitro showed prodrug **3** was greatly selectively toxic to tumor cells over-expressing NQO1, taxol-resistant A549, hypoxia A549 and HepG2, and lower damage to normal cells in comparison with podophyllotoxin, prodrug **1** and **2**. As elucidated by further mechanistic research, prodrug **3** was activated via NQO1 to efficiently while gently produce cytotoxic PPT units and kill tumor cells. In additions, in vivo study revealed that **3** significantly suppressed cancer growth in HepG2 xenograft models without obvious toxicity. Therefore, this NQO1-activatable prodrug delivery system exhibits good biosafety and provides a novel strategy for the development of drug delivery systems.

Keywords: Podophyllotoxin; NQO1-activatable prodrug; NQO1; Antitumor

1. Introduction

Naturally occurring substances account for the abundant sources to discover the anticancer drugs,[1] however, a number of antitumor naturally-occurring substances do not show target specificity, which may even show adverse toxicity to non-carcinoma cells. For reducing cytotoxicity and maintaining the treatment activity of those bio-active naturally occurring substances, appropriate structural modification may be adopted to be the vital way to develop drugs. Podophyllotoxin (PPT), one of the naturally occurring aryltetralin lignins, is separated based on plant podophyllum.[2] PPT, together with the derivatives, is suggested recently to show obvious anticancer effects.[3] Unfortunately, PPT shows high toxicity to non-carcinoma cells,[2] which hinders the development of it to antitumor agent. Moreover, it is of great challenge to lower PPT toxicity to non-carcinoma cells and maintain its toxicity against tumor cells.

Tumor-specic prodrugs can be accurately activated at cancer sites via species showing selectivity to tumor, like glutathione (GSH),[4,5] enzymes[6,7] and reactive oxygen species (ROS),[8,9] which can significantly improve the therapeutic efficacy of anticancer drugs. NAD(P)-H:quinone oxidoreductase-1 (NQO1, DT-diaphorase, EC 1.6.99.2) catalyzes the direct two electrons reduction for various quinones, with NADPH and NADH being the cofactors.[10] NQO1 is up-regulated within some human cancer tissues,[11-17] such as non-small cell lung carcinoma (NSCLC), pancreatic carcinoma (PCa), or colorectal cancer (CRC), as a result, it is a meaning target to activate quinone prodrugs or the fluorescent probes.[18-24] In this work, we designed and synthesized three NQO1-activatable PPT prodrugs which were constituted by an active drug PPT, a

different self-immolative linker, and a NQO1-responsive trigger group, respectively (Fig. 1). Based on the outcomes of preliminary tumor cell selection, compound **3** with the highest potency and selectivity was assessed for its ability of PPT release responding to NQO1, together with its antitumor effect and stability within plasma or buffers.

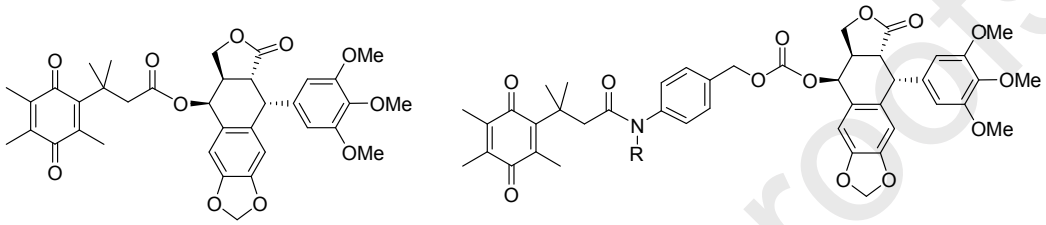

1

2, R = H
3, R= CH_3

Fig. 1. Structures for NQO1-activatable PPT prodrugs.

2. Results and discussion

2.1. Chemistry

Scheme 1 and 2 describe the synthetic routes for prodrugs **1**-**3**. Firstly, with dry methanesulfonic acid, trimethylhydroquinone **4** reacted with the 3,3-dimethylacrylic acid to yield **5**, and it was then subjected to N-bromosuccinimide (NBS) treatment within the aqueous acetone, finally yielding **6** (Scheme 1). Quinone unit **6** was coupled to PPT by EDCI, along with appropriate volume of DMAP for producing **1.** The syntheses of prodrugs **2** and **3** are shown in Scheme 2. Compound 6 was activated with isobutyl chloroformate and coupled with *p*-aminobenzylalcohol **7a** and *p*-methylaminobenzylalcohol **7b** for giving compounds **8a** and **8b**, respectively. Finally, compounds **8a** and **8b** were activated by 4-nitrophenyl chloroformate with DIPEA,

followed by treatment with PPT, to yield the prodrugs **2** and **3**, in parallel.

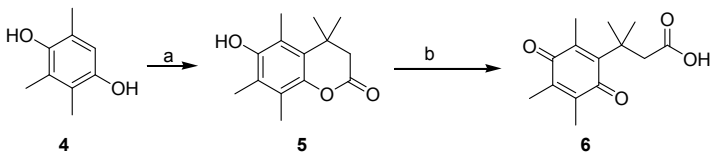

Scheme 1. Synthesis of **6**. Reagents and conditions: (a) 3,3-dimethylacrylic acid, CH_3SO_3H, 70 °C; (b) NBS.

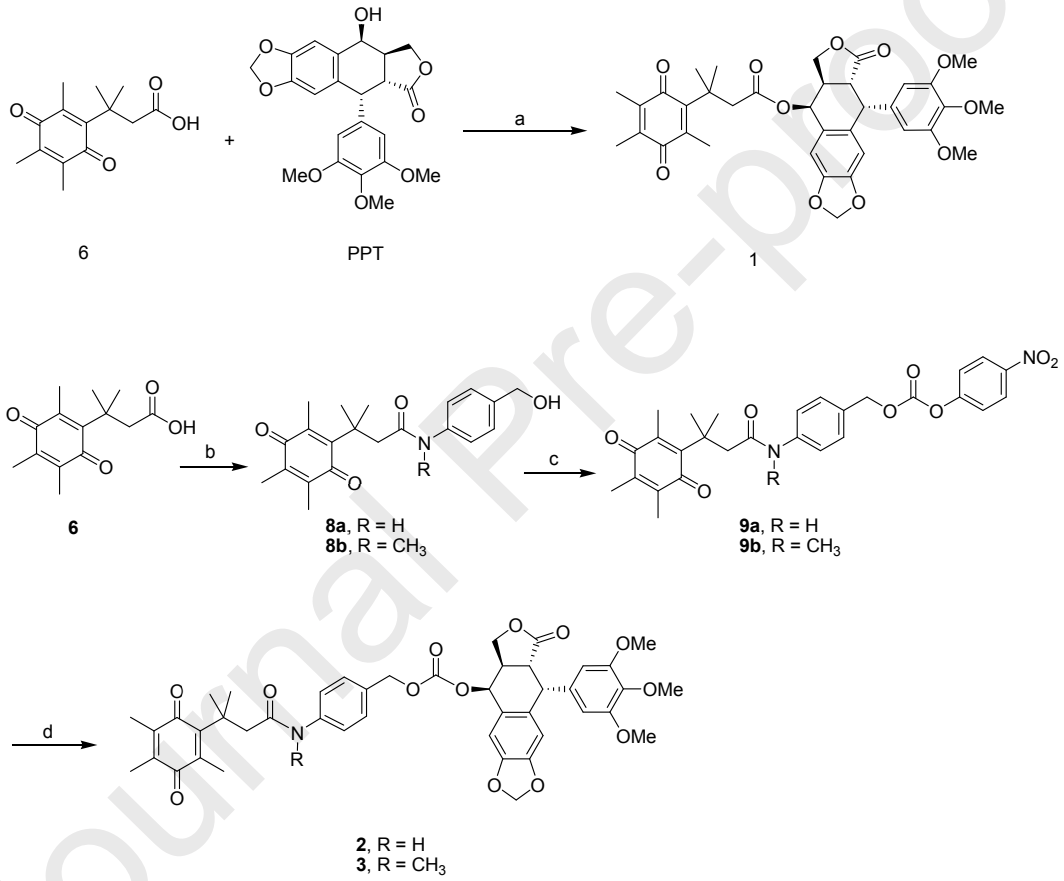

Scheme 2. Synthesis of prodrugs **1**-**3**. Reagents and conditions: (a) DCC, DMAP; (b) isobutyl chloroformate, p-aminobenzylalcohol (**7a**), p-methylaminobenzylalcohol (**7b**); (c) p-nitrobenzylchloroformate, DIPEA; (d) PPT, DMAP.

2.2. In vitro antiproliferative activity

After the synthesis of prodrugs **1**-**3**, five cell lines including NQO1-overexpressing

A549 and HepG2, hypoxia-induced A549 (A549/Hyp) and HepG2 (HepG2/Hyp), taxol-resistant A549 (A549/T), normal human liver LO2 cell lines were screened for better evaluating their antiproliferative effects. As shown in Table 1, prodrug **3** displayed the most potent activities against NQO1-overexpressing A549 and HepG2 cells, and IC_{50} values were 84 and 100 nM, respectively, which were comparable to those of PPT. In comparison, **1**-**2** were relatively less active toward the two cells. It was possibly because of the rapid reducibility of **3**, resulting in unfavorable degradation within the extracellular environment. As regards therapeutic range, compound **3** showed greater selectivity, normal liver cells in which NQO1 was not detected had the IC_{50} of 313 nM, which was 3.72 folds higher than the anti-HepG2 effect, while 3.67 folds greater than PPT (85 nM), suggesting that prodrug **3** showed a broad therapeutic index. In addition, compared with PPT, **3** had a significant inhibitory effect on A549/T cells, HepG2/Hyp and A549/Hyp cells. Based on the above research on antiproliferative activity, prodrug **3** of the most potent and selective was further evaluated its effect on PPT release responding to NQO1, stability within plasma or buffers, and the antitumor effect.

Table 1. The antiproliferative activities of PPT prodrugs **1-3.**

Compound.	IC_{50} (nM)					
	HepG2	A549	LO2	HepG2/Hyp	A549/Hyp	A549/T
1	107±11	160±14	228±36	193±14	315±44	302±33
2	262±29	274±39	452±33	425±32	596±70	574±50
3	84±9	100±19	312±34	113±13	185±24	197±29
PPT	83±8	105±15	85 ±11	209±16	291±25	338±38

2.3 Molecular modelling studies

Molecular modeling was carried out by the use of Autodock vina 1.1.2 for explaining how **3** was bound within NQO1 As a result, **3**'s quinone moiety bound to residues at NQO1 active site together with flavinadenine dinucleotide (FAD), and this was necessary for catalytic performance of NQO1 (Fig. 2). For PPT, its leaving groups were maintained out of binding pocket of substrates, which indicated that reaction between quinone and active site in NQO1 was unaffected by introducing PPT into quinone.

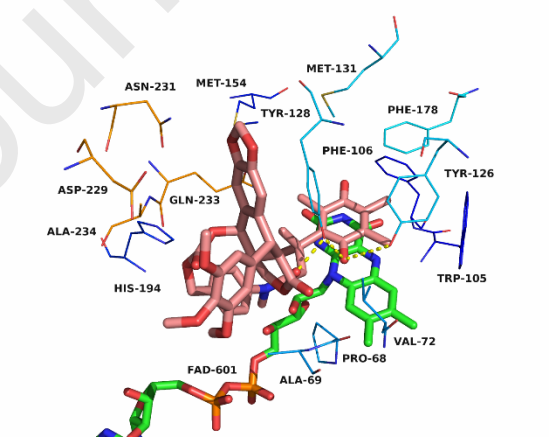

Fig. 2. Proposed binding model for prodrug **3** (orange) binding with NQO1.

2.4. In vitro drug release profiles of PPT

Prodrug **3** release profile responding to NQO1 and the cofactor NADPH was investigated through HPLC assay (Fig. 3A). We observed the prodrug release time dependence for prodrug **3** (Fig. 3B). As the incubation time increased, the PPT proportion showed a steady increase trend, with the plateau being observed at 9 h, reaching 83.4 %. To determine whether **3** was dependent on NQO1 for release, **3** was tested combined with dicoumarol (DIC, the NQO1 inhibitor). The results suggested that transformation of **3** into PPT was suppressed when DIC content increased to 50 μM. Then, the PPT formation within the recombinant NQO1 at different concentrations of the prodrug **3** was measured through HPLC assay. Later, the Michaelis−Menten curves were plotted, and the apparent Km and Vmax were 6.997 μM and 26.18 nmol/mg/min, respectively (Fig. 3C).

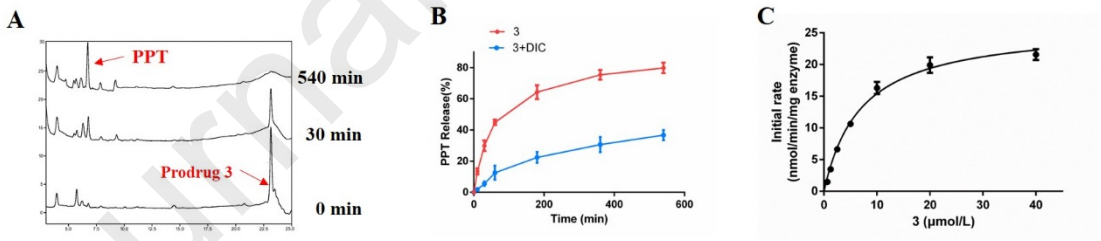

Fig 3. Prodrug **3** release profiles of PPT. (A) HPLC spectrum of **3** in the presence of NQO1. (B) PPT released from prodrug in the presence of NQO1(red), NQO1+DIC (blue) respectively. (C) Michaelis−Menten curves for **3** with NQO1.

A plausible process of PPT release from prodrug **3** is proposed in Fig. 4. To respond to the activation of NQO1 bioreduction, “trimethyl lock” that contained the trigger group of quinone propionic acid in **3** firstly underwent intramolecular cyclization, later,

linker was removed through the renounced 1,6-elimination reaction for the spontaneous liberation of PPT, thus specifically targeting tumor cells. Besides, HRMS assay was conducted to observe the expected PPT production (Fig. 5). Following the coincubation of **3** with NQO1 as well as NADPH, this study detected related fragments, such as PPT ($[M + Na]^+$ m/z =437.1291), **5** ($[M + Na]^+$ m/z = 257.1136) and **10** ($[M + H]^+$ m/z = 120.0808), which offered enough information for PPT delivery when there was NQO1.

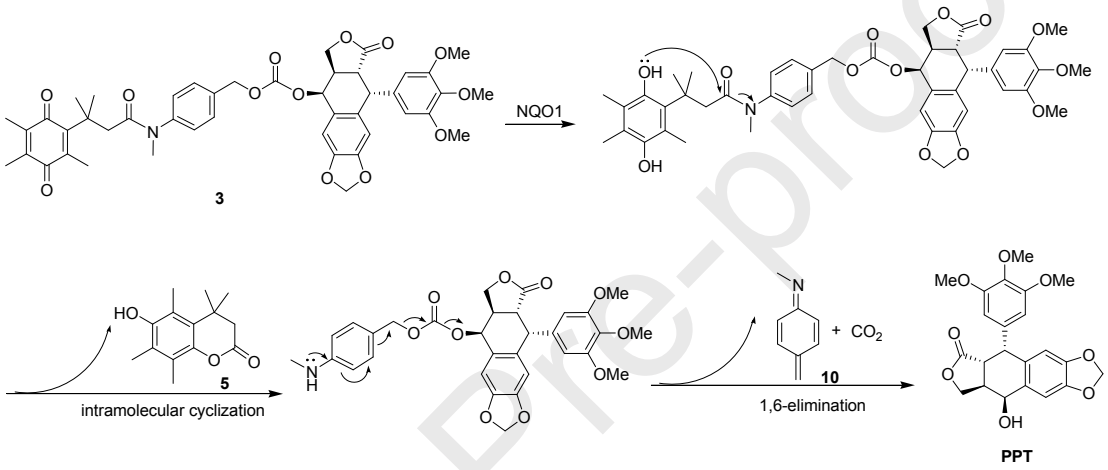

Fig. 4. A plausible process of PPT release from prodrug **3**.

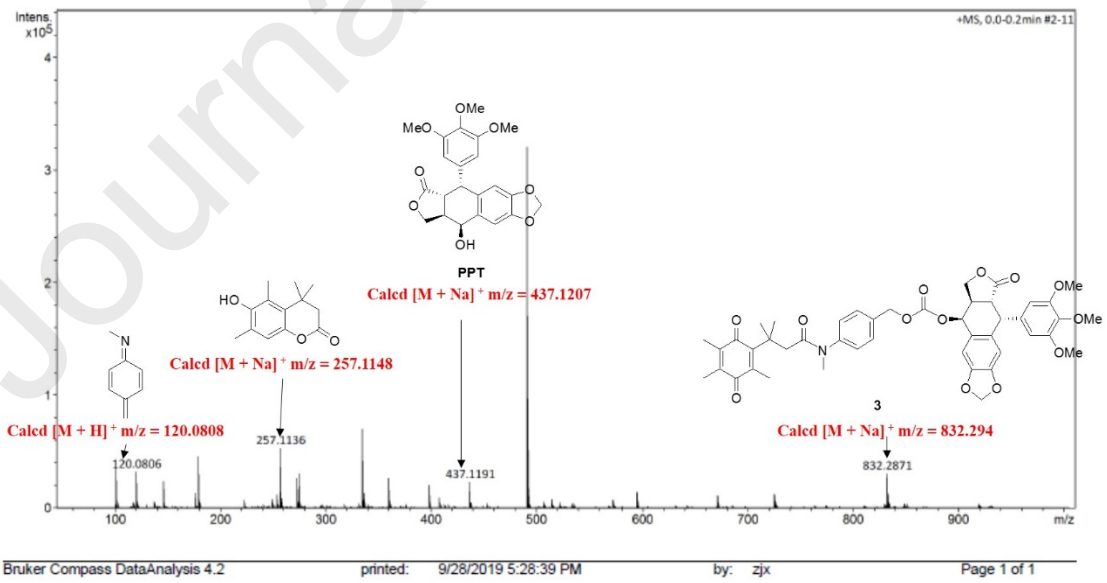

Fig. 5. HRMS analyses for **3** following co-incubation with NQO1 for 30 min.

*2.5. Stability of prodrug **3***

A majority of agents show no tissue specificity, and can be easily removed from liver and plasma. In this case, only a fraction of agents penetrate the site of treatment, leading to reduced efficacy. Prodrug **3** displayed good stability under 37 °C within the phosphate buffer (pH 5-9) in the presence of NADPH, rat plasma and human liver microsomes incubated for 9 h (Fig. 6). These findings indicated that **3** showed relative stability for providing sufficient exposure time at physiological conditions, as a result, **3** was targeted to produce cytotoxic substance into tumor tissue that over-expressed NQO1

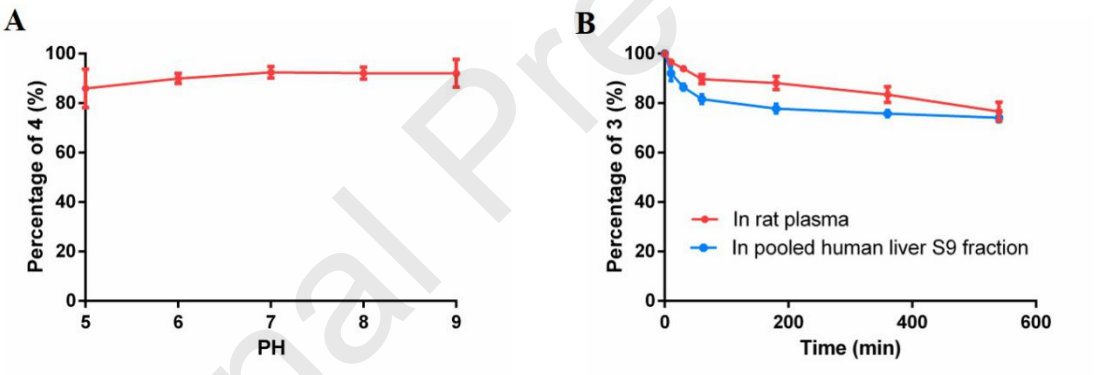

Fig. 6. The stability of prodrugs **3**. (A) in phosphate buffer. (B) in rat plasma (red) and human liver microsomes (blue).

2.6. Immunofluorescence and inhibition of microtubule assembly analysis

For investigating the effect of prodrug **3** on disrupting microtubular dynamics with alive cells, this study carried out immunofluorescent assay based on the HepG2 cells. According to Fig. 7, HepG2 cells of control group were arranged and organized normally. Nonetheless, when cells were treated with 50 nM **3** for 48 h, those microtubular networks within cytosol were destroyed, suggesting that **3** potentially

induced microtubular network collapse. To investigate whether the prodrug was related to the interactions with microtubule systems, **3** were evaluated as tubulin polymerization inhibitor. The results indicated that **3** had no inhibitory effects on the tubulin polymerization activity. Following co-incubation of prodrug **3** with NADPH and NQO1, the product was capable of inhibiting tubulin polymerization activity. These results provided sufficient evidence that NQO1 could facilitate the transformation of **3** into PPT which could effective inhibition microtubule assembly and showed the high antitumor activity.

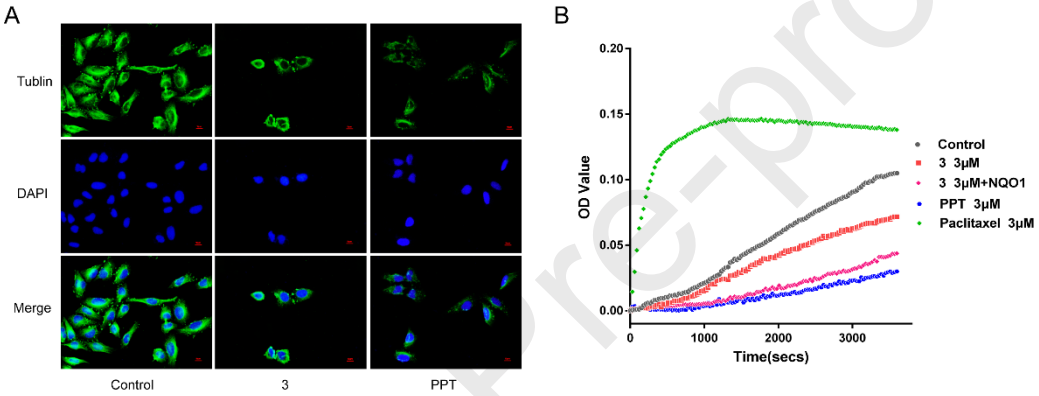

Fig. 7. (A) Effects of **3** on microtubule network organization, HepG cells were subjected to 48 h of DMSO, 50 nM of **3**, and 50 nM of PPT treatments. (B) Effects of **3** on tubulin polymerization in vitro.

2.7. Analysis of cell cycle

A majority of tubulin-destabilizing drugs might destroy distribution of cell cycle, this study conducted flow cytometric analysis for examining how **3** affected the progression of HepG2 cell cycle through staining with propidium iodide (PI). It was observed from Fig. 8 that, incubation with **3** resulted in cell cycle arrest at G2/M phase. In comparison with control cells subjected to DMSO incubation, HepG2 cells incubated using 50 nM **3** elevated the cell percentage at G2/M phase between 12.26% and 27.30%.

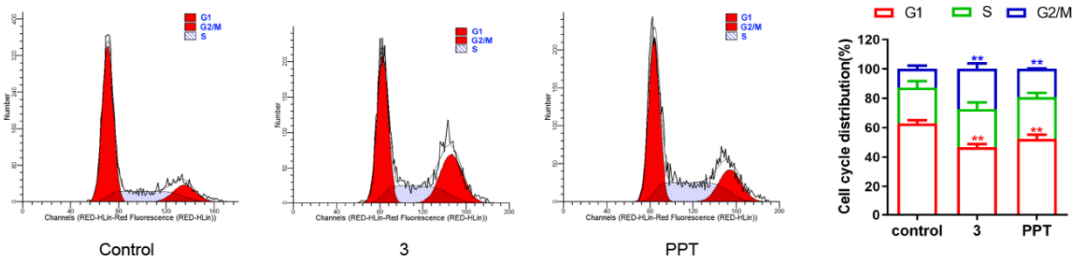

Fig. 8. 3 effects on the progression of HepG2 cell cycle. Cells were subjected to 24 h of **3** (50 nM) and PPT (50 nM) treatments.

2.8. Analysis of cell apoptosis

For assessing the effect of compound **3** on inducing cell apoptosis, this study conducted the Annexin V-FITC/PI assay. It was illustrated from Fig. 9 that, following 24 h treatment, the apoptotic cell percentage was as low as 3.40% of that of control group. After incubation using 50 nM **3** for 24 h, there were 17.5% apoptotic cells at the early or later stage. As suggested by the above findings, **3** could efficiently induce HepG2 cell apoptosis.

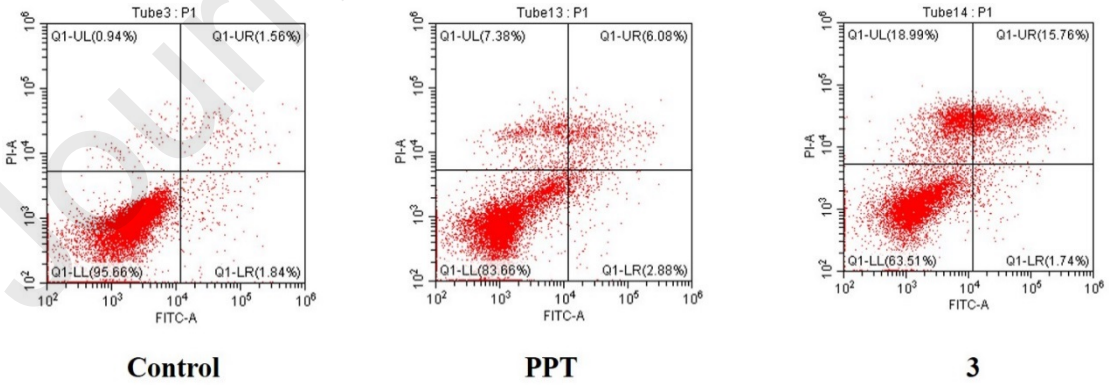

Fig. 9. Compound **3** led to apoptosis of HepG2 cells under **3** (50 nM) and PPT (50 nM) treatments.

2.9. Antitumor activity in vivo

In line with favorable observations of **3** in vitro, the efficacy of this compound in vivo to resist HepG2 xenograft was assessed using BALB/c nude mouse mode, with. PPT being the positive control. First, HepG2 cells were subcutaneously inoculated to mouse right flank to establish the mouse model of liver cancer allograft. When the tumor grew to a size of about 70-100 mm^3 and became palpable, all mice were randomly divided as blank, vehicle control or treatment group (with 6 in each group). Vehicle or drugs were administered intraperitoneal every other day for 17 consecutive days. Vehicle (5% DMSO + 40% PEG300 + 5% Tween 80 + 50% normal saline) was administered to control mice. PPT was administrated at the dosage of 10 mg/kg, and two different doses (10 and 5 mg/ kg) for **3** were studied. On day 17 following the initial administration, each mouse was sacrificed to harvest the tumor. Then, liver, heart, kidney, lung, and spleen and tumor tissues were sliced and stained using hematoxylin and eosin (H&E). Animals subjected to PPT treatment died in the experimental period, which might be due to the high toxicity of PPT. Relative to vehicle group, intraperitoneal injection with 10 mg/kg **3** markedly reduced tumor growth. Upon the completion of our observation, it inhibited tumor growth up to 64% (Fig. 10A-C). Moreover, **3** had no significant effect on body weight, even at 10 mg/kg (Fig. 10D). Then, the standard H&E staining protocol was applied in histologically examining liver, heart, lung, kidney spleen and tumor tissues. Under light microscope, the morphology and structure of these tissues were normal and showed no significant histological damage as compared with that in the control (Fig 11). The above results suggested that, compound **3** was successfully designed to decrease PPT cytotoxicity in vivo, which might be potentially used as the antitumor drug with low toxicity.

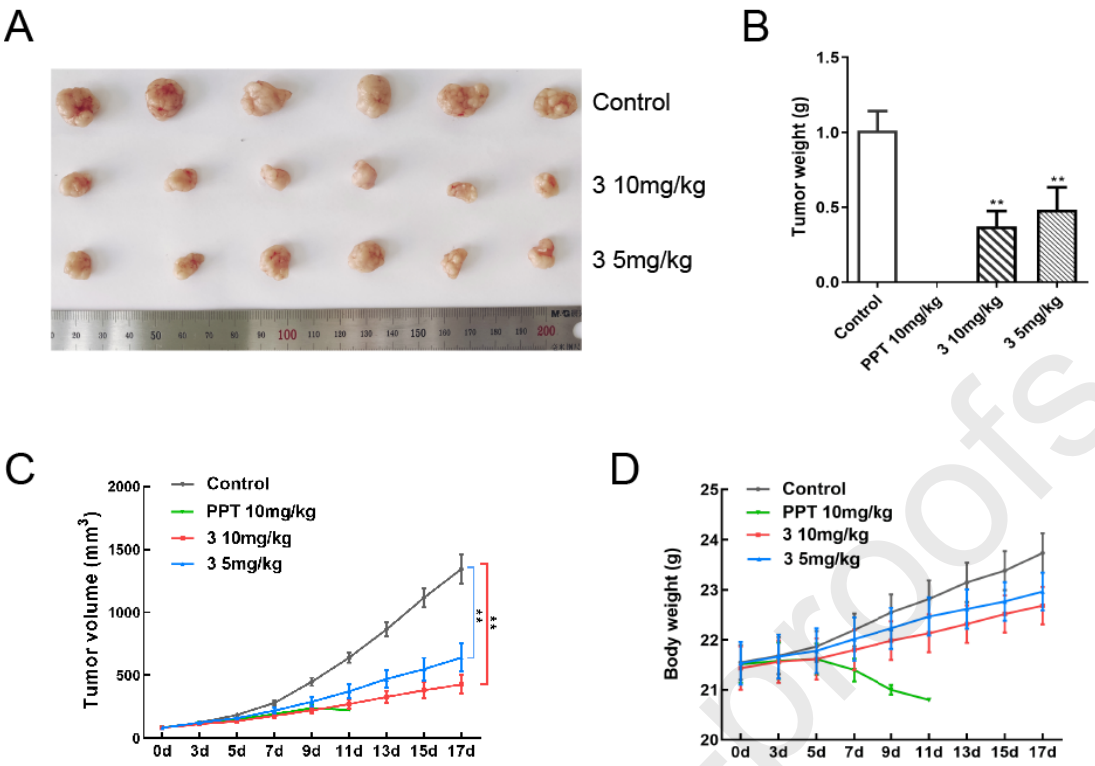

Fig.10. 3 suppressed the growth of liver cancer xenograft in vivo. Following vehicle, PPT (10 mg/kg/two day), **3** (10 mg/kg/ two day) and **3** (5 mg/kg/two day) treatments for 17 consecutive days, all animals were sacrificed to harvest and weigh the tumors. (A) Tumor images acquired from mice on 17 days following treatment initiation. (B) The excised tumor weights in each group. compared with control group. (C) Changes in mouse tumor volume in the treatment process. (D) Changes in mouse body weight in the process of treatment. **P <0.01 vs. Control.

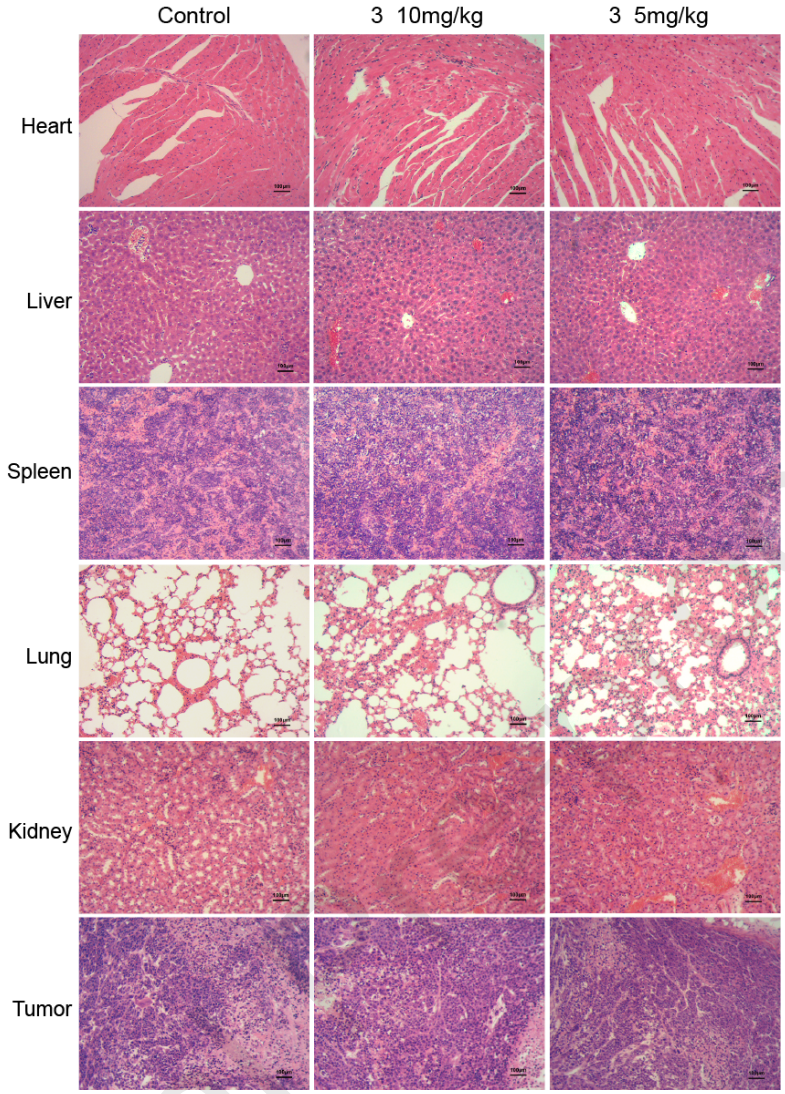

Fig. 11. Representative images of heart, liver, spleen, lung, kidney tissues and tumor stained by H&E .

3. Conclusions

To sum up, this study introduces a novel successful design for converting the naturally occurring PPT with high toxicity to the potential antitumor agent with low toxicity. The antiproliferative activities in vitro showed prodrug **3** was greatly selectively toxic to tumor cells over-expressing NQO1, taxol-resistant A549, hypoxia A549 and HepG2, and lower damage to normal cells in comparison with ppt, prodrug

1, **2** and **3**. Further mechanism studies elucidated that the NQO1 activates prodrug **3** in a bioreductive way, followed by intramolecular cyclization as well as 1,6-elimination reaction, thus efficiently liberating parent drug PPT. In additions, as indicated by in vivo anticancer assessment, the prodrug **3** exerted the stronger anticancer effect and the higher safety than PPT.

4. Experimental section

4.1. Chemiistry

4.1.1. General

The 98% PPT was provided by Macklin Inc. (Shanghai, China). Recombinant NQO1 (DT-diaphorase) with the purity of >90% was provided by Sigma-Aldrich China Co., Ltd. (Shanghai, China). Compound **5** and **8** were prepared according to literature.[25] The remaining reagents were purchased from commercial sources. Melting points were determined with a XT-4 binocular microscope and are uncorrected. The ^{1}H NMR and ^{13}C NMR spectra were measured on a Bruker AV-400 instrument using deuterated solvents with tetramethylsilane (TMS) as internal standard. High resolution mass spectra (HRMS) were recorded on a Bruker micrOTOF-QIII mass spectrometer. The ACS Accurasil C18 column (dimension, 4.6 mm × 150 mm, 5 μm) was utilized for HPLC analysis by the use of the solvent acetonitrile /water mixture at the 0.5 mL/min flow rate, and the UV absorption was observed at the wavelength of 292 nm.

*4.1.2. Synthesis of prodrug **1***

A mixture containing **5** (140 mg, 0.6 mmol), EDCl (115mg, 0.6mol) and CH_2Cl_2 (10 mL) was incubate at 0 ^{o}C. After stirring for 30min, 6 mg DMAP (0.05 mmol) and 207 mg PPT (0.5 mmol) were put into the resultant mixture for 24 h reaction under ambient temperature. After reaction completion, the mixed product was rinsed by the $NaHCO_3$

saturated solution together with brine. Then, anhydrous Na_2SO_4 was used for drying the solvent. After filtration, evaporation in vacuum was conducted to concentrate the organic solvent, and column chromatography was conducted to purify the crude products, with petroleum ether/ethyl acetate (v:v=2:1) being used to be the eluent, for yielding 293 mg (51%) yellow power, m.p.102-103 ^oC; ^1H NMR (400 MHz, DMSO-d_6) δ: 6.75 (s, 1H), 6.60 (s, 1H), 6.32 (s, 1H), 6.02 (d, 2H, J = 10 Hz), 5.82 (d, 1H, J = 10 Hz), 4.54 (d, 1H, J = 4.4 Hz), 4.20-4.08 (m, 2H), 3.65 (s, 6H), 3.62 (s, 3H), 3.36-3.31 (m, 1H), 3.12 (d, 1H, J = 16.4 Hz), 2.99 (d, 1H, J = 16.4 Hz), 2.75-2.67 (m, 1H), 2.10 (s, 3H), 1.89 (s, 3H), 1.86 (s, 3H), 1.43 (s, 3H), 1.42 (s, 3H); ^{13}C NMR (100 MHz, DMSO-d_6) δ: 190.7, 187.2, 174.3, 173.1, 152.5 (2C), 152.3, 147.8, 147.4, 142.7, 139.3, 138.6, 136.9, 136.1, 132.7, 129.1, 109.9, 108.5 (2C), 106.9, 101.9, 73.3, 70.9, 60.4, 56.2 (2C), 47.6, 44.5, 43.3, 38.6, 38.2, 29.0 (2C), 14.5, 12.8, 12.3; HRMS-ESI (m/z): calcd for $C_{36}H_{38}NaO_{11}$ $[M+Na]^+$ 669.2306, found: 669.2308.

4.1.3. Synthesis of compound ***9***

Compound **8** (1 mmol) was dissolved in dry CH_2Cl_2 (30 mL), and 4-nitrophenyl chloroformate (425 mg, 2 mmol) was added. To the above solution, DIPEA (260 mg, 2 mmol) was added dropwise. The resultant mixture was kept stirring for 6 h at room temperature. After completion of the reaction, 100 mL water was used to wash the reaction solution for thrice, and anhydrous Na_2SO_4 was used for drying. Later, solvent was discarded, silica gel column chromatography was performed to purify the residue on, with petroleum ether/ethyl acetate (v:v=3:1) being used to be the eluent for obtaining compound **9**.

N-(4-(hydroxymethyl)phenyl)-3-methyl-3-(2,4,5-trimethyl-3,6-dioxocyclohexa-1,4-dienyl)butanamide (**9a**). Compound **9a** was prepared from **8a** as a yellow solid, m.p.127-128 ^oC, yield 69%, m.p.127-128 ^oC. ^1H NMR (400 MHz, $CDCl_3$) δ: 8.19 (d, J

= 7.2 Hz,2H), 7.38 (d, *J* = 8.4 Hz,2H), 7.29 (d, *J* = 8.4 Hz,4H), 7.15 (s, 1H), 5.16 (s, 2H), 2.97 (s, 2H), 2.09 (s, 3H), 1.89 (s, 3H), 1.88 (s, 3H), 1.42 (s, 6H); ^{13}C NMR (100 MHz, $CDCl_3$) *δ*: 190.6, 186.5, 169.4, 154.5, 151.7, 151.4, 144.3, 142.1, 137.5, 137.4, 137.3, 128.8, 128.7 (2C), 124.3 (2C), 120.8 (2C), 118.8 (2C), 69.6, 49.4, 37.4, 28.1 (2C), 13.2, 11.7, 11.2; HRMS-ESI (m/z): calcd for $C_{28}H_{28}N_2NaO_8$ $[M+Na]^+$ 543.1738, found: 543.1747.

N-(4-(hydroxymethyl)phenyl)-N,3-dimethyl-3-(2,4,5-trimethyl-3,6-dioxocyclohexa-1,4-dienyl)butanamide (**9b**). Compound **9a** was prepared from **8a** as a yellow oil, yield 68%**,** ^{1}H NMR (400 MHz, $CDCl_3$) *δ*: 8.29 (d, *J* = 9.2 Hz, 2H), 7.55 (d, *J* = 8.0 Hz, 2H), 7.43 (d, *J* = 9.2 Hz, 2H), 7.28 (d, *J* = 8.0 Hz, 2H), 5.36 (s, 2H), 3.18 (s, 3H), 2.78 (s, 3H), 2.11 (s, 3H), 2.01 (s, 3H), 1.96 (s, 3H), 1.42 (s, 6H); ^{13}C NMR (100 MHz, $CDCl_3$) *δ*: 191.2, 187.6, 172.0, 155.4, 154.6, 152.4, 145.4, 144.5, 143.5, 137.8, 136.3 (2C), 133.9, 130.1 (2C), 127.9, 125.3 (2C), 121.8 (2C), 70.1, 47.7, 38.1, 37.1, 28.5 (2C), 14.1, 12.7, 12.1; HRMS-ESI (m/z): calcd for $C_{29}H_{30}N_2NaO_8$ $[M+Na]^+$ 557.1900, found: 557.1890.

*4.1.4. Synthesis of prodrug **2***

Compound **9a** (520 mg, 1 mmol) and DMAP (122 mg, 1 mmol) were dissolved in dry CH_2Cl_2 (20 mL), then added PPT ((414 mg, 1 mmol), and the reaction mixture was stirred for overnight at room temperature. Later 50 mL was used to wash reaction mixture for twice, and then organic layer was isolated, followed by drying with anhydrous Na_2SO_4. Later, rotary evaporation was performed to remove solvents, column chromatography was applied on silica gel to purify crude product, with petroleum CHCl3/ethyl acetate (v:v=10:1) being used to be the eluent for yielding compound 2 (382 mg, 48%) as a yellow oil. ^{1}H NMR (400 MHz, $CDCl_3$) *δ*: 7.44 (d, 2H, *J* = 8.4 Hz), 7.33 (d, 2H, *J* = 8.4 Hz), 7.19 (s, 1H),6.84 (s, 1H), 6.53 (s, 1H), 6.37

(s, 2H), 5.98 (s, 2H), 5.74 (dd, 1H, *J* = 3.2, 7.2 Hz), 5.14 (s, 2H), 4.60 (d, 1H, *J* = 2.0 Hz), 4.44-4.40 (m, 1H), 4.24-4.19 (m, 1H), 3.80 (s, 3H), 3.74 (s, 6H), 3.04 (s, 2H), 2.92 (d, 2H, *J* = 3.2 Hz), 2.16 (s, 3H), 1.95 (s, 3H), 1.94 (s, 6H), 1.49 (s, 6H); ^{13}C NMR (100 MHz, $CDCl_3$) *δ*: 191.6, 187.5, 173.6, 170.4, 155.4, 152.6 (2C), 148.3, 147.7, 143.2, 138.5, 138.2, 137.0, 134.6, 132.3, 129.5 (2C), 127.6, 127.4, 126.2, 119.8 (2C), 115.6, 109.7, 107.9 (2C), 107.2, 101.6, 71.2, 69.9, 60.8, 56.1 (2C), 50.5, 45.5, 43.7, 38.4, 29.7, 29.1 (2C), 19.0, 14.2, 12.7, 12.2; HRMS-ESI (m/z): calcd for $C_{44}H_{45}NNaO_{13}$ $[M+Na]^+$ 818.2783, found: 818.2784.

4.1.6. Synthesis of prodrug 3

Compound **9b** (534 mg, 1 mmol) and DMAP (122 mg, 1 mmol) were dissolved in dry CH_2Cl_2 (20 mL), then added PPT ((414 mg, 1 mmol), and the reaction mixture was stirred for overnight at room temperature. Later 50 mL was used to wash reaction mixture for twice, and then organic layer was isolated, followed by drying with anhydrous Na_2SO_4. Later, rotary evaporation was performed to remove solvents, column chromatography was applied on silica gel to purify crude product, with petroleum CHCl3/ethyl acetate (v:v=10:1) being used to be the eluent for yielding compound 2 (382 mg, 48%) as a yellow soild, m.p.115-116 ^{o}C. ^{1}H NMR (400 MHz, $CDCl_3$) *δ*: 7.49 (d, 2H, *J* = 7.6 Hz), 7.25 (d, 2H, *J* = 7.6 Hz), 6.87 (s, 1H), 6.55 (s, 1H), 6.39 (s, 2H), 5.99 (d, 2H, *J* = 1.6 Hz), 5.80 (d, 1H, *J* = 7.6 Hz), 5.30 (s, 2H), 4.61 (d, 1H, *J* = 3.2 Hz), 4.48-4.44 (m, 1H), 4.28-4.23 (m, 1H), 3.80 (s, 3H), 3.78 (s, 6H), 3.17 (s, 3H), 2.99-2. 92 (m, 2H), 2.76 (s, 2H), 2.11 (s, 3H), 2.00 (s, 3H), 1.94 (s, 3H), 1.31 (s, 6H); ^{13}C NMR (100 MHz, $CDCl_3$) *δ*: 191.3, 187.7, 173.5, 172.1, 155.4, 154.5, 152.7 (2C), 148.4, 147.7, 144.4, 143.4, 138.0, 137.2, 136.5, 134.6, 134.4, 132.4, 129.8, 127.8, 127.5, 126.1, 115.5, 109.8 (2C), 108.1, 107.1, 101.7, 77.7, 71.2, 69.5, 60.8, 56.2 (2C), 53.4, 47.8, 45.5, 43.7, 38.4, 38.1, 28.5 (2C), 14.1, 12.7, 12.1; HRMS-ESI (m/z): calcd

for $C_{45}H_{48}NaO_{13}$ $[M+Na]^+$ 810.312, found: 810.3123.

4.2. Antiproliferative experiment

The A549, HepG2, A549/Hyp, HepG2/Hyp, A549/T cells, and normal LO2 cells were used to test compound anti-proliferative effects. The logarithmic cells were inoculated into the 96-well plates for adherence, followed by 48 h of incubation using compounds at specific doses. After adding MTT, cells were further incubated for 2-3 h. Later, MTT formazan crystal was mixed into DMSO, and absorbance (A) was detected at 570 nm.

4.3. Molecular modeling studies

NQO1 crystal structure in the complex containing a coumarin-based inhibitor (PDB code 3JSX) was used for docking study. Then, ligand was eliminated, leaving the receptor complex in later docking study, followed by the geometrical addition of polar hydrogen atoms into protein. AutoDock Tools were utilized to assign docking regions. The default parameters were applied in Vina docking, except as otherwise specified. This study selected the optimal-scoring pose determined based on Vina docking score, while PyMoL 1.7.6 (http://www.pymol.org/) was used for visual analysis.

*4.4. HPLC and HRMS assays for drug **3** release studies*

HPLC was used to determine the activation of prodrug, with NQO1 being the stimulus (eventual dose of 10 μg/mL). Incubation mixtures contained 10 mM PBS with 2 % tween 80, 100 μM NADPH, and 20 μM prodrug **3**. Recombinant NQO1 was directly put to the incubation mixtures for reaction initiation and then the solution was incubated at 37 ^oC for appropriate time intervals. The reaction was terminated by adding cold acetonitrile (100 μL). After centrifugation in a refrigerated centrifuge, 20 μL of the liquid were loaded and analyzed by HPLC and HRMS analysis. To investigate the DIC effect, NQO1 was previously incubated using 50 μM DIC for 20 min.

4.5. Formation rates of CA-4 in recombinant NQO1 from PPT

The rate of NQO1 catalysis were calculated during the first 30 min to determine the susceptibility of the prodrugs **3** on target enzyme NQO1. The assay mixtures contained NADPH (100 μM), recombinant human NQO1 (10 μg/mL) and **3** (40, 20, 10, 5, 2.5, 1.25, 0.625 μM) within 100 μL PBS (10 mmol , pH 7.4) with 2 % tween 80. 30 min of reactions were conducted under 37 ^{o}C, and 100 μL cold acetonitrile was added to terminate reactions. After centrifugation in a refrigerated centrifuge, 20 μL of the liquid were loaded and analyzed by HPLC. Enzymatic variables (K_m along with V_{max}) were determined based on kinetic curves using GraphPad Prism 7.0.

*4.6. Stability study of **3***

HPLC was conducted for examining prodrug **3** stability in PBS buffer with different pH values, in rat plasma and pooled Human Liver S9 Fraction. The assays were performed at 37 °C and conducted in triplicate.

Stability of prodrug **3** in PBS buffer with different pH values: In the absence of NQO1, the prodrug (10 μM) was co-incubated with cofactor NADPH (100 μM) in PBS with 2 % tween 80 at different pH values. After incubation for appropriate time intervals, the reaction was terminated by adding cold acetonitrile (100 μL). After centrifugation in a refrigerated centrifuge, 20 μL of the liquid were loaded and analyzed by HPLC.

Metabolic Stability in plasma: Rat plasma were subjected to vortex mixing and then centrifugation for 5 min at 10000 rpm to deproteinize and the resulting supernatants were withdrawn, prodrug **3** (10 μM) was co-incubated with supernatants with 2 % tween 80 at 37 °C for 0, 10, 30, 60, 1800, 360 and 540 min. After centrifugation in a refrigerated centrifuge, 20 μL of the liquid were loaded and analyzed by HPLC.

Metabolic Stability in pooled Human Liver S9 Fraction: The metabolic stability was performed in 10 mmol M PBS (pH 7.4) containing 2 % tween 80, **3** (10 μM) and pooled

Human Liver S9 Fraction (0.5 mg) at 37 °C. The reaction was started by adding 100 μM NADPH and terminated at 0, 10, 30, 60, 1800, 360 and 540 min by adding 100 μL cold acetonitrile . After centrifugation in a refrigerated centrifuge. 20 μL of the liquid were loaded and analyzed by HPLC with UV detection under 292 nm.

4.7. Cell cycle analysis

HepG2 cells were first of all inoculated into the 12-well plates for 24 h, followed by 24 h incubation after **3** treatment. Then, cells were harvested and rinsed by cold PBS for two times, followed by 3 h suspension within the 70% ethanol. Following addition of 5 mL RNase A (10 mg/mL), the suspension was subjected to 1 h incubation under ambient temperature. Subsequently, 10 mL PI (50 mg/mL) was also put into the suspension. At last, cell proportions at diverse cell cycle phases were measured by flow cytometry..

4.8. Cell apoptosis analysis

The Annexin-V FITC/PI assay was conducted to evaluate the apoptotic effect of prodrug **3**. First of all, the HepG2 cell line was cultivated into the 6-well plates for 24 h incubation. Thereafter, the original medium was replaced with the complete medium supplemented with **3** (50 nM) to incubate for another 24 h. Later, supernatant was collected to obtain cells through trypsinization, which were subjected to PBS washing, 15 min Annexin-V/FITC (5 mL) staining within PBS under ambient temperature, and 10 min staining using PI solution. The apoptosis levels were evaluated by flow cytometry.

4.9. Immunofluorescence staining

HepG2 were inoculated into the 96-well plate to incubate under 37 ^{o}C for 12 h under 5% CO_2 condition. Later, cells were subjected to 48 h DMSO, PPT, and **3** treatments, separately, methanol fixation as well as 0.5% Triton X-100/PBS permeabilization.

Then, cells were carried out overnight incubation using the α-tubulin primary antibody under 4 ^{o}C. Following PBS washing, cells were subjected to 1 h incubation using related fluorescence-labeled secondary immunofluorescence staining antibody. Later, DAPI was used to label cell nucleus, and the fluorescence microscope was utilized for visualization.

4.10. Tubulin polymerization test

The tubulin polymerization test was conducted in accordance with manufacturer's instructions using the tubulin polymerization kit (BK004P, Cytoskeleton). Absorbance were recorded for 1 h at 340 nm wavelength every 30 seconds, to obtain the kinetic curves of polymerization and depolymerization of microtubules. The reaction groups for these experiments included: vehicle control, **3** (3 μM), **3** (3 μM) + NQO1, PPT (3 μM) and Paclitaxel (3 μM).

4.11. In vivo antitumor effect

HepG2 cells were utilized to investigate the antitumor effect of **3** within the BALB/c nude mice. The BALB/c nude mice (6 weeks old) were provided by Vital River Laboratory Animal Technology Co. Ltd. Then, 5×10^6 HepG2 cells contained within the 100 mL sterile PBS were subcutaneously injected into the dorsal regions of mice to induce tumor. When the tumor grew to 70-100 mm^3, the animals were randomLy separated as 4 groups (with 6 in every group): control, 10 mg/kg PPT, 5/10 mg/kg **3**, and the compounds were administrated every other day for 17 days by intraperitoneal injection. All the compounds were prepared with the formulation in 5% DMSO, 40% PEG 300, 5% tween-80 and 50% saline. Body weight as well as tumor volume was measured at an interval of 2 days following prodrug treatment, among which, the latter was recorded using calipers through determining length (A) and width (B) for calculation according to the formula $V = AB^2/2$. In addition, tumor weight was

measured and tumor growth inhibition rate was calculated upon treatment completion. Liver tissue samples were obtained following execution, which were then subjected to 4% paraformaldehyde fixation, ethanol dehydration, paraffin embedding, followed by HE staining and microscopic observation.

Acknowledgements

This work was supported by NSFC-Henan Joint Fund (No. U1604164) and the Doctoral Scientific Research Activation Foundation of Xinxiang Medical University (No. XYBSKYZZ201906)

Appendix A. Supplementary data

Supplementary data to this article can be found online at

References

1. Newman, D.J.; Cragg, G.M. Natural products as sources of new drugs over the last 25 years. *J. Nat. Prod.* **2007**, *70*, 461–477.
2. Gordaliza, M.; García, P.A.; Miguel del Corral, J.M.; Castro, M.A.; Gómez-Zurita, M.A. Podophyllotoxin: distribution, sources, applications and new cytotoxic derivatives. *Toxicon* **2004**, *44*, 441−449.
3. Gordaliza, M.; Castro, M.A.; Corral, J.M.M.; San Feliciano, del A. Antitumor properties of podophyllotoxin and related compounds. *Current Pharm. Design* **2000**, *6*, 1811-1839.
4. Liu, Y.; Zhu, S.; Gu, K.; Guo, Z.; Huang, X.; Wang, M.; Amin, H.M.; Zhu, W.; Shi, P. GSH-activated NIR fluorescent prodrug for podophyllotoxin delivery. *ACS Appl. Mater. Interfaces* **2017**, *9*, 29496−29504.
5. Maiti, S.; Park, N.; Han, J.H.; Jeon, H.M.; Lee, J.H.; Bhuniya, S.; Kang, C.; Kim, J.S. Gemcitabine-coumarin-biotin conjugates: A target specific theranostic anticancer prodrug. *J. Am. Chem. Soc.* **2013**, *135*, 4567–4572.

6. Schellmann, N.; Deckert, P.M.; Bachran, D.; Fuchs, H.; Bachran, C. Targeted enzyme prodrug therapies. *Mini-Rev. Med. Chem*. **2010**, *10*, 887-904.
7. Liu, P.; Xu, J.; Yan, D.; Zhang, P.; Zeng, F.; Li, B.; Wu, S.A. DT-diaphorase responsive theranostic prodrug for diagnosis, drug release monitoring and therapy, *Chem. Commun.* **2015**, *51*, 9567-9570.
8. Ou, K.; Kang, Y.; Chen, L.; Zhang, X.; Chen, X.; Zheng, Y.; Wu, J.; Guan, S. H_2O_2-responsive nano-prodrug for podophyllotoxin delivery. *Biomater. Sci*. **2019**, *7*, 2491–2498.
9. Redy-Keisar, O.; Ferber, S.; Satchi-Fainaro, R.; Shabat, D. NIR fluorogenic dye as a modular platform for prodrug assembly: real-time in vivo monitoring of drug release. *ChemMedChem* **2015**, *10*, 999-1007.
10. Siegel, D.; Gustafson, D.L.; Dehn, D.L.; Han, J.Y.; Boonchoong, P.; Berliner, L.J.; Ross, D. NAD(P)H: quinone oxidoreductase 1: role as a superoxide scavenger. *Mol. Pharmacol*. **2004**, *65*, 1238-1247.
11. Yang, Y.; Zhang, Y.; Wu, Q.; Cui, X.; Lin, Z.; Liu, S.; Chen, L. Clinical implications of high NQO1 expression in breast cancers. *J. Exp. Clin. Cancer Res*. **2014**, *33*, 14.
12. Awadallah, N.S.; Dehn, D.; Shah, R.J. NQO1 expression in pancreatic cancer and its potential use as a biomarker. *Appl. Immunohisto. M. M.* **2008**, *16*, 24–31.
13. Yang, Y.; Zhang, Y.; Wu, Q.Y.; Cui, X.L.; Lin, Z.H.; Liu, S.P.; Chen, L.Y. Clinical implications of high NQO1 expression in breast cancers. *J. Exp. Clin. Cancer Res*. **2014**, *33*, 1–9.
14. Belinsky, M.; Jaiswal, A.K. NAD (P) H: quinone oxidoreductase1 (DT-Diaphorase) expression in normal and tumor tissues. *Cancer Metastasis Rev*. **1993**, *12*, 103-117.

15. Cresteil, T.; Jaiswal, A.K. High levels of expression of the NAD(P)H: Quinone oxidoreductase (NQO1) gene in tumor cells compared to normal cells of the same origin. *Biochem. Pharmacol*. **1991**, *42*, 1021-1027.
16. Smitskamp-Wilms, E.; Giaccone, G.; Pinedo, H.M.; van der Laan, B.F.; Peters, G.J. DT-diaphorase activity in normal and neoplastic human tissues; an indicator for sensitivity to bioreductive agents? *Br. J. Cancer* **1995**, *72*, 917–921.
17. Mikami, K.; Naito, M.; Ishiguro, T.; Yano, H.; Tomida, A.; Yamada, T.; Tanaka, N.; Shirakusa, T.; Tsuruo, T. Immunological quantitation of DT-diaphorase in carcinoma cell lines and clinical colon cancers: advanced tumors express greater levels of DT-diaphorase. *Jpn. J. Cancer Res*. **1998**, *89*, 910-915.
18. Zhang, K.; Chen, D.; Ma, K.; Wu, X.; Hao, H.; Jiang, S. NAD(P)H: Quinone oxidoreductase 1 (NQO1) as a therapeutic and diagnostic target in cancer. *J. Med. Chem*. **2018**, *61*, 6983-7003.
19. Danson, S.; Ward, T.H.; Butler, J.; Ranson, M. DT-diaphorase: a target for new anticancer drugs. *Cancer Treat. Rev*. **2004**, *30*, 437-449.
20. Mendoza, M.F.; Hollabaugh, N.M.; Hettiarachchi, S.U.; McCarley, R.L. Human NAD(P)H:quinone oxidoreductase type I (hNQO1) activation of quinone propionic acid trigger groups. *Biochemistry* **2012**, *51*, 8014-8026.
21. Zhang, X.; Li, X.; Li, Z.; Wu, X.; Wu,Y.; You, Q.; Zhang, X. An NAD(P)H: Quinone oxidoreductase 1 responsive and self-immolative prodrug of 5-fluorouracil for safe and effective cancer therapy. *Org. Lett*. **2018**, **20**, 3635−3638.
22. Suebsakwong, P.; Wang, J.; Khetkam, P.; Weerapreeyakul, N.; Wu, J.; Du, Y.; Yao, Z.-J.; Li, J.-X.; Suksamrarn, A. A Bioreductive prodrug of cucurbitacin B significantly inhibits tumor growth in the 4T1 xenograft mice model. *ACS Med. Chem. Lett.* **2019**, *10*, 1400-1406.

23. Liu, P.; Xu, J.; Yan, D.; Zhang, P.; Zeng, F.; Li, B.; Wu, S. A DT-diaphorase responsive theranostic prodrug for diagnosis, drug release monitoring and therapy. *Chem. Commun*. **2015**, *51*, 9567-9570.

24. Liu, M.; Song, W.; Du, X.; Su, J.; Dong, K.; Chen, Y.; Peng, Z. NQO1-selective activated prodrug of triptolide: Synthesis and antihepatocellular carcinoma activity evaluation. *ACS Med. Chem. Lett*. **2018**. *9*, 1253-1257.

25. Zhou, W.; Leippe, D.; Duellman, S.; Sobol, M.; Vidugiriene, J.; O'Brien, M.; Shultz, J.W.; Kimball, J.J.; DiBernardo, C.; Moothart, L.; Bernad, L.; Cali, J.; Klaubert, D.H.; Meisenheimer, P. Self-immolative bioluminogenic quinone luciferins for NAD(P)H assays and reducing capacity-based cell viability assays. *Chembiochem*. **2014**, *15*, 670-675.

Highlights

►Three NQO1-activatable podophyllotoxin prodrugs were synthesized

► Prodrug **3** had highly selective toxicity to cancer cells and lower damage to normal cells

► Prodrug **3** could be activated by NQO1 and effectively liberate podophyllotoxin and kill tumor cells.

► Prodrug **3** exerted a stronger anticancer activity and a more favorable safety profile in vivo

Graphical abstract

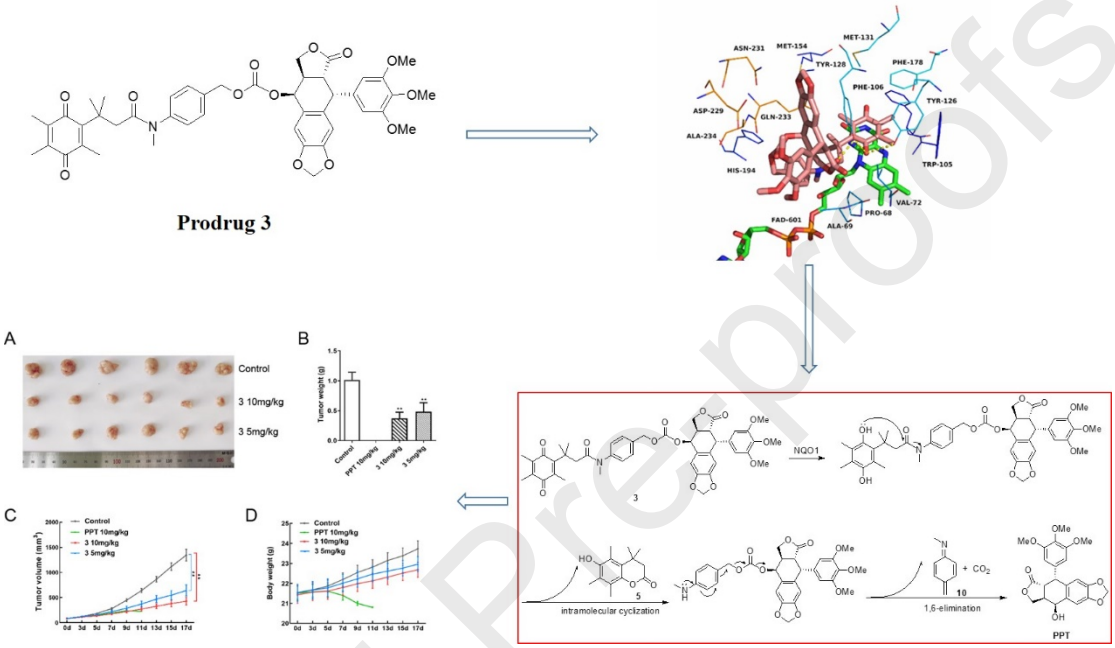

Declaration of interests

☒ The authors declare that they have no known competing financial interests or personal relationships that could have appeared to influence the work reported in this paper.

☐The authors declare the following financial interests/personal relationships which may be considered as potential competing interests: